Title
FTO controls reversible m6Am RNA methylation during snRNA biogenesis

Permalink
https://escholarship.org/uc/item/89j7p21g

Authors
Mauer, Jan
Sindelar, Miriam
Despic, Vladimir
et al.

Peer reviewed

FTO controls reversible m6Am RNA methylation during snRNA biogenesis

Jan Mauer[1,†], **Miriam Sindelar**[1,#], **Vladimir Despic**[1,#], **Théo Guez**[2], **Ben R. Hawley**[1], **Jean-Jacques Vasseur**[2], **Andrea Rentmeister**[3], **Steven S. Gross**[1], **Livio Pellizzoni**[4], **Françoise Debart**[2], **Hani Goodarzi**[5], **Samie R. Jaffrey**[1,*]

[1]Department of Pharmacology, Weill Cornell Medicine, Cornell University, New York, NY 10065, USA.

[2]IBMM, Université de Montpellier, CNRS, ENSCM, Montpellier, France.

[3]Department of Chemistry, Institute of Biochemistry, University of Muenster, Muenster, Germany.

[4]Department of Pathology and Cell Biology, Center for Motor Neuron Biology and Disease, Columbia University, New York, New York, USA.

[5]Department of Biochemistry and Biophysics, University of California, San Francisco, San Francisco, California, USA.

Summary

Small nuclear RNAs (snRNAs) are core spliceosome components and mediate pre-mRNA splicing. Here we show that snRNAs contain a regulated and reversible nucleotide modification causing them to exist as two different methyl isoforms, m_1 and m_2, reflecting the methylation state of the adenosine adjacent to the snRNA cap. We find that snRNA biogenesis involves the formation of an initial m_1-isoform with a single-methylated adenosine (2'-*O*-methyladenosine, Am), which is then converted to a dimethylated m_2-isoform (N^6,2'-*O*-dimethyladenosine, m^6Am). The relative m_1- and m_2-isoform levels are determined by the RNA demethylase FTO, which selectively demethylates the m_2-isoform. We show FTO is inhibited by the oncometabolite D-2-hydroxyglutarate, resulting in increased m_2-snRNA levels. Furthermore, cells that exhibit high m_2-snRNA levels show altered patterns of alternative splicing. Together, these data reveal that FTO controls a previously unknown central step of snRNA processing involving reversible methylation, and suggest that epitranscriptomic information in snRNA may influence mRNA splicing.

[*]Corresponding author. srj2003@med.cornell.edu.
[†]present address: BioMed X Innovation Center, 69120 Heidelberg, Germany
[#]equal contribution

Small nuclear RNAs (snRNAs) are among the most abundant and extensively studied RNAs in eukaryotes. These uridine (U)-rich non-coding RNAs – which include U1, U2, U4, U5, and U6 – were discovered nearly fifty years ago[1], and studies of their function lead to the elucidation of the fundamental molecular mechanisms that mediate pre-mRNA splicing[2,3].

snRNAs undergo a series of processing events that are required for incorporation into spliceosomes. Except for U6 and U6atac snRNA[4], snRNAs are synthesized by RNA polymerase II as precursors that initially contain a 3'-end extension and acquire an N^7-methylguanosine (m^7G) cap (ref. 5). snRNAs are exported into the cytosol where they are incorporated into small nuclear ribonucleoproteins (snRNPs) by binding to Sm proteins[6]. Their m^7G cap is then further methylated to form the $N^{2,2,7}$-trimethylguanosine (TMG) cap and the snRNA 3'-end is trimmed[7–9]. snRNAs are incorporated into snRNPs and then transported back to the nucleus where they assemble into spliceosomes that mediate pre-mRNA splicing[10–12]. snRNAs that are not properly processed are not incorporated into snRNPs and are therefore unstable and degraded[13,14].

Importantly, snRNAs contain a set of constitutive nucleotide modifications that are highly conserved across species and essential for snRNA integrity and function[15,16]. Thus, all mature snRNAs are thought to exist as a single molecular species, and deviations outside of this species are not thought to be utilized by spliceosomes.

Recent data suggests that nucleotide modifications may be susceptible to demethylation reactions, based on the studies of fat mass and obesity-associated protein (FTO)[17]. However, it has been difficult to identify endogenous substrates of FTO. FTO exhibits weak demethylase activity towards N^3-methyluridine (m^3U) and N^6-methyladenosine (m^6A) (ref. 17,18). We recently showed that FTO highly efficiently demethylates $N^6,2'$-O-dimethyladenosine (m^6Am), with nearly 100-fold higher catalytic activity towards m^6Am compared to m^6A (ref. 19). FTO selectively demethylates the N^6-methyl, resulting in 2'-O-methyladenosine (Am) (ref. 19). m^6Am is exclusively found within the "extended cap" of RNA polymerase II-transcribed RNAs, at the transcription-start nucleotide immediately adjacent to the m^7G (ref. 20,21).

Studies of FTO have primarily focused on mRNA. However, direct biochemical demonstration that a specific m^6A or m^6Am site in mRNA is regulated by FTO is missing. Since m^6A and m^6Am are present at high stoichiometry in mRNA, they appear to evade demethylation by FTO[19]. Indeed, nearly all the m^6Am peaks in mRNA showed increases of less than 10% in *Fto* knockout brain compared to wild-type[19]. The moderate effect of FTO depletion on m^6A or m^6Am levels in mRNA likely reflects the fact that mRNAs are predominantly cytosolic[19] while FTO is nuclear in most cells and tissues[17,22]. Thus, we previously proposed that the endogenous target of FTO may by nuclear RNA rather than mRNA[19].

Here we show that all Sm-class spliceosomal snRNAs can exist as two distinct isoforms, differing by a single methyl modification on the adenosine residue that is located at the transcription-start nucleotide of most snRNAs. This adenosine has previously been annotated to contain a constitutive 2'-O-methyl modification on the ribose sugar[15,23]. We

find that these adenosines are subjected to a second, reversible methylation selectively at the N^6-position on the adenine base. This methylation converts the canonical single-methylated m_1-snRNA to a dimethylated m_2-snRNA. These m_2-snRNAs are major targets of FTO, which functions early during snRNA biogenesis to convert the m_2-snRNA back to m_1-snRNA. FTO-mediated demethylation of m_2-snRNA is blocked by the oncometabolite D-2-hydroxyglutarate, linking intracellular metabolism to snRNA methylation state. Upon FTO inhibition, m_2-snRNAs accumulate and are assembled into snRNPs, which is correlated with enhanced splicing of exons that are normally poorly included. Overall these data reveal the presence of an FTO-regulated methylation switch that enables the formation of previously unrecognized methyl isoforms of snRNA. Our findings point to m^6Am in snRNAs as the major target of FTO and the potential for FTO and cellular metabolites to influence transcriptome diversity by controlling the reversible methylation of snRNA.

Results

The RNA demethylase FTO selectively demethylates snRNAs

To identify FTO targets, we used the miCLIP approach, which involves N^6-methyladenine (6mA) antibodies (which bind both m^6A and m^6Am) that are UV-crosslinked to purified RNA. After stringent washing, antibody-bound RNA is subjected to next generation sequencing to identify 6mA-modified nucleotides[24]. We used miCLIP to map 6mA in wild-type and *Fto*-knockout mouse liver RNA (Supplementary Fig. 1a). Unlike in previous studies[22,25], no poly(A) purification was used, thus allowing all cellular RNAs to be analyzed. To detect m^6Am, we searched for RNA species that show increased methylation at the transcription-start nucleotide (TSN) in the *Fto* knockout transcriptome compared to wild type.

Although many RNAs showed potential methylation differences at the TSN (Fig. 1a, grey circles), the vast majority did not pass the applied filters and their methylation change did not reach statistical significance after multiple comparison testing. However, a small subset of methylation events was significantly increased in the *Fto* knockout transcriptome (Fig. 1a, orange dots, adjusted *P*-value < 0.05). These RNAs were exclusively small nuclear RNAs (snRNAs), including U1, U4atac, and U5. In each case, the miCLIP signal was associated with read terminations at the TSN, suggesting that the first nucleotide contains an N^6-methyl modification.

We next looked at the methylation fold change of Sm- and Lsm-class snRNAs. We observed increased TSN methylation of all Sm-class snRNAs of the major and minor spliceosome (Fig. 1b, Supplementary Fig. 1b). In each case, the 6mA reads were detected around the TSN and were between 10–20-fold higher in the *Fto* knockout compared to wildtype (Fig. 1c, Supplementary Figs. 2a–h).

In addition to snRNAs, several snRNA-like transcripts showed markedly increased 6mA reads in the *Fto* knockout transcriptome. These include U7, which is involved in 3'-end processing of histone mRNAs[26] and the small nucleolar RNAs (snoRNAs) U3 and U8, which function in rRNA processing (Supplementary Figs. 3a–c). U3 and U8 snoRNAs are unusual in that they are not derived from intronic sequences, but instead transcribed from

their own gene by RNA polymerase II using a promoter that contains sequence elements typical for snRNA genes[27]. No other snoRNAs exhibited significantly elevated 6mA reads in the *Fto* knockout.

The increase in 6mA reads was seen in all Sm-class snRNAs, but not the Lsm-class snRNAs U6 and U6atac – the only two spliceosomal snRNAs that are transcribed by RNA polymerase III (ref. 4) (Fig. 1b, Supplementary Figs. 1b, 2g,h). U6 and U6atac do not acquire an m7G cap; however, U6 snRNA contains an internal m6A (ref. 15,28). Nevertheless, and in contrast to a recent report[29], FTO depletion did not lead to a statistically significant alteration in 6mA reads at this internal position (Supplementary Figs. 2g and 4a).

Similarly, U2, which contains an internal m6Am (ref. 15, see also modomics.genesilico.pl), did not show a robust increase of 6mA reads at this position (Supplementary Fig. 2a). Notably, U1 snRNA, which is thought to not contain m6A or m6Am at internal sites based on 6mA immunoprecipitation experiments and biochemical modification mapping[28,30,31], was recently suggested to contain m6Am at a previously undocumented internal site[29]. However, no significant enrichment of miCLIP reads was detected at this site in *Fto* knockout liver (Supplementary Fig. 4b).

miCLIP does not distinguish between mature snRNA and the unprocessed longer snRNA precursors or truncated forms. Therefore, we used 6mA immunoblotting to detect the length of 6mA-immunoreactive snRNAs. In these experiments, we immunoblotted small RNA (<200 nt) from wild-type and *FTO* knockout HEK293 cells. We observed bands corresponding to the mature snRNA forms, with significantly increased 6mA-immunoreactivity in *FTO* knockout cells (Fig. 1d).

Overall, the miCLIP results indicate that the FTO-regulated sites are specifically localized to the TSN region of Sm-class snRNAs and all Sm-class snRNAs are substrates for FTO-mediated demethylation.

The first nucleotide of snRNAs is reversibly methylated

The finding that Sm-class snRNA modification is regulated by FTO was surprising, since these snRNAs are not known to contain m6Am or m6A at the TSN. Instead, Sm-class snRNAs are thought to contain 2'-*O*-methyladenosine (Am) at this position[8]. Since the miCLIP results suggest that the first nucleotide in snRNAs in *FTO* knockout cells are either m6A or m6Am, we determined its identity using a thin-layer chromatography (TLC)-based assay[21]. In this assay, the 5'-cap is removed, followed by radiolabeling of the exposed 5' nucleotide with [γ–^{32}P]-ATP. Next, the snRNAs are treated with ribonuclease and the nucleotide hydrolysate is resolved by 2D-TLC. This approach readily identifies the first nucleotide based on its migration pattern[21].

We first examined the small RNA fraction (<200 nt), which is highly enriched in snRNAs. In wild-type cells, the first nucleotide was predominantly Am, with low, but measurable levels of m6Am (Fig. 2a). However, small RNAs prepared from *FTO* knockout HEK293 cells exhibited a pronounced increase in the level of m6Am at the first nucleotide (Fig. 2a).

We next directly measured the first nucleotide in gel-purified U1 and U2, which migrate to well-defined positions by PAGE (Figs. 1d, 2b). Consistent with previous publications[8], the first nucleotide in U1 and U2 was predominantly Am in wild-type HEK293 cells (Fig. 2b,c). However, in *FTO*-knockout cells, m^6Am was markedly increased, with levels similar to Am (Fig. 2b,c).

U2 is difficult to analyze by miCLIP since it contains a constitutive internal m^6Am which causes this snRNA to be immunoprecipitated irrespective of the methylation status of its TSN (Supplementary Fig. 2a). The TLC analysis directly demonstrates that U2 also contains an m^6Am nucleotide that is regulated by FTO (Fig. 2c).

We next developed a mass spectrometry-based assay to examine m^6Am or Am specifically in the context of the cap structure. Small RNA was treated with P1 nuclease, resulting in all internal nucleotides being digested to mononucleotides. Under these conditions, the first nucleotide remains connected to the cap in the form of a "cap-dinucleotide" structure (cap-ppp-Am or cap-ppp-m^6Am) (Supplementary Fig. 5a).

Cap-dinucleotides were readily quantified by high-resolution mass spectrometry using positive ion-mode detection, since negative ion mode did not allow sensitive detection (Supplementary Fig. 5b). A multiple reaction monitoring protocol was developed based on the fragment ion transitions from distinct dinucleotide precursor species (Supplementary Fig. 5c). This approach exhibited high sensitivity and linear detection of cap dinucleotides, thus revealing the first nucleotide within the cap context (Supplementary Fig. 5d).

We verified that Am was associated with the cap after digestion of small RNA from wild-type HEK293 cells (Fig. 2d). However, m^6Am was the predominant form in *FTO*-knockout HEK293 cells, with a 6.3-fold enrichment of m^6Am over Am (Fig. 2d). Thus, both TLC and mass spectrometry indicate that snRNAs contain m^6Am at the first nucleotide in FTO-deficient cells.

Together, these results suggest that during snRNA biogenesis, snRNAs undergo methylation to form a readily detectable dimethylated form (m_2-snRNA) with m^6Am as the first nucleotide. The m_2-snRNA can then be demethylated by FTO to a single-methylated snRNA (m_1-snRNA) with Am as the first nucleotide.

m_2-snRNAs are detected in different cells and tissues

To determine the prevalence of m_2-snRNAs in cells that are not genetically depleted of FTO, we isolated small RNAs and assayed the TSN by mass spectrometry from various cells and tissues. In brain, only m_1-snRNAs were detected (Fig. 2e). However, in liver, HEK293 cells, mouse embryonic stem cells (mESCs), HT1080 fibrosarcoma and TF-1 erythroleukemia cells, m_2-snRNAs were readily detected at 1–15% of the level of m_1-snRNAs (Fig. 2e and Supplementary Figs. 6b–e). UOK262 renal cell carcinoma cells, which exhibit elevated fumarate due to fumarate hydratase deficiency[32], showed ~3-fold higher m_2-snRNA to m_1-snRNA ratio than HEK293 cells (Supplementary Fig. 6c).

We next asked if the levels of m_1-snRNAs and m_2-snRNAs are regulated during embryonic stem cell development. To test this, we cultured mESCs for five days in the presence or

absence of differentiation inhibitors. Mass spectrometry revealed a two-fold increase in m_2-snRNAs upon removal of differentiation inhibitors (Supplementary Figs. 6d,e).

Together, these data indicate that m_2-snRNAs are nearly undetectable in many cells and tissues, but can be readily detected in others and can be induced in response to certain stimuli.

m_2-snRNAs increase in response to 2-hydroxyglutarate

FTO is inhibited by natural metabolites and oncometabolites, including citrate, succinate, fumarate, and D-2-hydroxyglutarate (2-HG)[33,34]. These metabolites compete with α-ketoglutarate, an FTO co-substrate, for demethylation[33].

Cancer-associated mutants of isocitrate dehydrogenase (IDH) generate high levels (>10 mM) of 2-HG[35]. To determine if 2-HG affects snRNA methylation, we first measured m_1-snRNAs and m_2-snRNAs levels in small RNA isolated from TF-1 cells expressing IDH1[R132H] and IDH2[R140Q] mutants[36,37]. In control cells, m_1-snRNAs predominated as the major first nucleotide in small RNA. However, m_2-snRNAs were markedly elevated following expression of both IDH1[R132H] and IDH2[R140Q], in proportion to the increase in intracellular 2-HG levels (Figs. 3a–c and Supplementary Figs. 7a,b). Notably, this effect was blocked by mutant isoform-selective small molecule inhibitors, indicating that the formation of m_2-snRNAs in 2-HG-dependent pathogenic conditions is reversible (Figs. 3a–c and Supplementary Figs. 7a,b).

We also tested the effects of dimethylfumarate, a pro-drug that is converted to fumarate in cells. Treatment of HEK293 cells for 7 days with 70 μM dimethylfumarate, a concentration used to study the cellular effects of this compound[38], did not significantly affect m_2-snRNA levels (Supplementary Fig. 7c). Thus, dimethylfumarate is unlikely to mediate its clinical effects by increasing levels of m_2-snRNAs.

Taken together, these data indicate that m_2-snRNA levels can be altered by 2-HG, and suggest the possibility that 2-HG-dependent pathogenic conditions are associated with increased levels of m_2-snRNAs.

m^6Am is demethylated prior to cap hypermethylation

snRNAs biogenesis involves an initial nuclear phase in which snRNA contain an m^7G cap, and a second nuclear phase, which occurs after cytoplasmic processing, and is marked by the presence of a TMG cap on snRNAs[7]. Since FTO is predominantly nuclear[17], the conversion of m_2-snRNAs to m_1-snRNAs by FTO likely takes place during one of these two nuclear phases.

We therefore chemically synthesized RNA substrates mimicking the pre-export and post-import cap structure of snRNA. These 20-nucleotide long RNAs started with either an m^7G or a TMG cap, followed by a triphosphate linker, and m^6Am. As described previously[19], FTO efficiently demethylated m^6Am in m^7G-capped RNA, as measured by formation of Am (Fig. 4a). However, FTO did not detectably demethylate m^6Am when using the post-import

RNA substrate comprising m^6Am with a TMG cap (Fig. 4a). These data suggest that m_2-snRNAs are not a substrate for FTO after TMG cap formation.

Based on the m^7G cap-specific demethylation and considering the nuclear localization of FTO, we infer the decision to demethylate m_2-snRNAs and form m_1-snRNAs is determined during the initial nuclear phase, after snRNA transcription but prior to cytoplasmic formation of the TMG cap and assembly of snRNPs.

m_2-snRNAs acquire a TMG cap and assemble into snRNPs

To test if m_2-snRNAs assemble into snRNPs, we immunoprecipitated snRNPs from cellular extracts using a small ribonucleoprotein particle protein B (SmB)-specific antibody. This approach has previously been shown to immunoprecipitate assembled snRNPs[39,40]. We then determined the first nucleotide of snRNAs in cellular snRNPs to determine if m_2-snRNAs are present. As expected, in control HEK293 cells, m_1-snRNAs were predominant (Fig. 4b). However, in *FTO* knockout HEK293 cells, m_2-snRNAs were readily detected (Fig. 4b). Thus, m_2-snRNAs form a distinct m^6Am-containing class of snRNPs, i.e. m_2-snRNPs.

After incorporation of snRNAs into snRNPs, their m^7G cap is modified to form the TMG cap[9]. We asked if m_2-snRNAs are similarly methylated to form the TMG cap using mass spectrometry. The small RNA fraction was purified from *FTO* knockout HEK293 cells and *Fto*-knockout mouse liver and brain. The RNA was digested with nuclease P1 to liberate the cap and m^6Am as the dinucleotide cap structure (cap-ppp-m^6Am). The presence of m^7G or TMG was then assessed in the liberated cap structure. In each case, the primary cap structure was the TMG cap attached to m^6Am (TMG-ppp-m^6Am) (Fig. 4c). This indicates that m_2-snRNAs undergo normal cap hypermethylation during their biogenesis.

Taken together, these data show that m_2-snRNAs undergo normal biogenesis, including incorporation into snRNPs and acquisition of the TMG cap structure.

Altered splicing is associated with m_2-snRNAs

We next sought to examine splicing changes upon FTO depletion. Similar to a previous study[41], we found that the most pronounced effect of FTO deficiency is increased exon inclusion (Supplementary Fig. 8a). To further refine this analysis, we characterized the included exons for binding sites of known splicing factors in a previously published RNA-Seq analysis using control and *FTO* knockout HEK293 cells[42]. Here, we observed a significant and specific enrichment for SRSF1, HNRNPH2 and HNRNPK-dependent exons, whereas enrichment of other exons was not detected (Supplementary Figs. 8b and 9a). Similar effects were also seen in our HEK293T *FTO* knockdown RNA-Seq dataset (Supplementary Fig. 9b). Thus, FTO depletion is associated with the enhanced inclusion of exons that would normally be inefficiently spliced into mature mRNA.

We next wanted to determine how m^6Am affects snRNAs, and if any of these changes are consistent with altered splicing phenotypes. In the case of mRNAs, DCP2-mediated mRNA degradation is impaired when m^6Am is present at the first nucleotide[19]. However, northern blotting of cellular RNA harvested from *DCP2* knockout HEK293 cells, which primarily

contain m_1-snRNAs, showed no increase in snRNAs relative to wild-type cells (Supplementary Fig. 10a). Thus, DCP2 does not appear to regulate m_1-snRNAs.

When we examined our own and pre-existing[42] RNA-Seq datasets from FTO-depleted cells, we observed moderately increased levels of some (e.g. U1, U4, and U5), but not all, Sm-class snRNA transcripts (Supplementary Figs. 10b–f).

Surprisingly, many genes encoding Lsm-class snRNAs (i.e. U6 and U6atac) showed increased expression (Supplementary Figs. 10b,c). U6 and U6atac lack m^6Am since they do not have adenosine at the first transcribed nucleotide, and show no alteration in 6mA levels in their transcript body in *FTO* knockout cells based on miCLIP (Supplementary Figs. 2g,h). Although U6 and U6atac do not contain m^6Am, they assemble into multiple distinct complexes with FTO-regulated Sm-class snRNPs. The increase in U6 snRNA levels in FTO-deficient cells may therefore be the consequence of altered interactions of U6 with m_2-snRNPs compared to m_1-snRNPs. Overall, these data demonstrate that FTO deficiency indirectly increases levels of U6, which could therefore impact splicing.

Discussion

A major class of cellular noncoding RNA are the snRNAs, which get assembled into ribonucleoproteins and have central roles in RNA processing reactions such as pre-mRNA splicing. Although snRNAs are often regulated by trans-acting splicing factors that modulate the association of snRNPs to specific transcripts, the modified nucleotides in snRNAs have not previously been thought to be the target of regulation. Here we show that snRNAs contain a regulated nucleotide methylation switch that allows them to exist as either of two distinct methylation isoforms. This methyl modification is located at the adenosine of the first encoded nucleotide in mRNA, is reversible, and is correlated with enhanced snRNA abundance and altered splicing profiles in cells. Together, our studies provide evidence that reversible epitranscriptomic information is encoded at the first nucleotide of snRNAs and that the reversible and regulated methylation of this nucleotide by FTO is a key aspect of snRNA biogenesis.

Our study focused on snRNA biogenesis and identified the formation of m_2-snRNAs and its subsequent demethylation to m_1-snRNA as a previously unknown step in snRNA maturation (Supplementary Fig. 11). snRNA biogenesis was extensively studied and involves Sm core assembly, 3' processing, nucleotide modifications at internal sites and formation of the hypermethylated guanosine cap[6,9–12,15]. Although Sm-class snRNAs were known to contain a 2'-*O*-methyl modification at the evolutionarily conserved starting-adenosine, our data reveal that snRNA biogenesis also involves a previously unrecognized N^6-methylation of this nucleotide. We find that the N^6-methyl modification is subsequently removed by FTO, thus converting m_2-snRNAs to m_1-snRNAs. Our studies reveal that FTO is an snRNA biogenesis factor, and snRNA biogenesis involves reversible methylation of the extended snRNA cap.

Our studies shed light on the physiologic substrate of FTO. Previous studies have focused on mRNA, and it has been argued that the high levels of m^6A may make it a relevant substrate

for FTO despite the weak demethylation activity observed for m^6A compared to the less abundant m^6Am[43,44]. However, any relevant substrate for FTO should in fact be in low abundance or undetectable, not high abundance, in FTO-expressing cells. Indeed, we show that m^6Am is very low in abundance in snRNA in most cells until FTO depletion. Given the high levels of snRNA in cells, the total cellular levels of m^6Am are markedly increased upon FTO depletion. Unlike m^6Am whose stoichiometry was directly quantified in specific snRNAs, m^6A has not been similarly shown to be regulated by FTO at any specific site by quantitative biochemical measurements of m^6A stoichiometry. Without this data, it remains unclear if FTO can directly demethylate specific m^6A residues in mRNA at a meaningful level.

FTO was previously shown to influence alternative splicing. These splicing changes were initially attributed to FTO-regulated m^6A residues around splice-sites. However, a role for m^6A in alternative splicing has recently been challenged[45]. Our findings potentially provide a resolution by showing that FTO regulates m^6Am in spliceosomal snRNAs. Thus, our discovery of FTO-regulated m_2-snRNAs provides the first direct link between FTO activity and the mRNA splicing machinery.

The decision to demethylate the m_2-snRNA appears to be determined early in snRNA biogenesis. We find that FTO-mediated demethylation of m_2-snRNAs is inhibited when 2-HG levels are increased due to expression of a cancer-associated mutant IDH. FTO was previously shown to be inhibited by metabolites that compete with α-ketoglutarate, including citrate, succinate, fumarate and 2-HG[33,34]. Our studies raise the possibility that 2-HG and potentially other metabolite abnormalities may mediate their effects, in part, by inhibiting FTO and increasing the levels of m_2-snRNAs that could in turn influence specific snRNA-mediated mRNA processing or splicing events.

The presence of m_2-snRNAs is not restricted to cells that lack FTO or express mutant IDH. We also detected m_2-snRNAs in mouse embryonic stem cells, TF-1 cells and mouse liver tissue by miCLIP and mass spectrometry. It will be important to determine the full spectrum of cell type-specific regulation of m_2-snRNA expression *in vivo* as well as whether different levels of m_2-snRNAs accumulate in cells because of FTO inhibition or due to other mechanisms.

How does the N^6-methyl modification affect the fate of snRNA? The N^6-methyl modification is unlikely to affect snRNA:pre-mRNA hybridization steps since these hybrids mostly occur at internal sites in the snRNA. For example, U1 snRNA hybridizes to the 5' splice site using nucleotides 3–7 (ref. 46). Instead, the methyl modification may affect the interactions of snRNA with other complexes. Splicing involves dynamic assembly and disassembly of U6 and U6atac snRNPs with Sm-class snRNPs[47]. It is intriguing to speculate that the altered U6 levels reflects differences in the dynamics of m_1- and m_2-snRNP complex assembly with U6. This may be mediated by dedicated reader proteins that alter the overall assembly, disassembly or turnover of multi- m_2-snRNP complexes. These alterations may in turn account for the increase in U6 snRNA levels. Therefore, it will be important to monitor the dynamics of multi-m_1- and m_2-snRNP complexes and to determine the transcriptome-wide binding properties of m_2-snRNPs.

Notably, recent studies showed that the levels of individual types of snRNAs can have large effects on splicing efficiency[48], and reduced snRNA expression is associated with severe splicing abnormalities[44,49]. The increased expression of U6 and some Sm-class snRNAs associated with FTO-deficiency may influence splicing patterns by specifically promoting the inclusion of exons that are otherwise inefficiently spliced due to rate-limiting availability of individual snRNPs or their higher order snRNP complexes.

Although snRNAs were previously thought to be comprised of a single molecular species, the demonstration that snRNAs exist as distinct methyl isoforms indicates a potential regulatory role for methylation switches in splicing. Importantly, some snRNAs have non-splicing functions[26,50] and their m_2-isoforms are likely to influence other RNA processing pathways. We suspect phenotypes linked to altered expression of FTO reflect alterations in these diverse snRNA-regulated RNA processing pathways. More research will be needed to understand the diversity of RNA processing alterations associated with m_2-snRNAs.

Methods

miCLIP-based mapping of 6mA and RNA-Seq analysis.

For miCLIP experiments, total RNA was extracted from *Fto* knockout mouse livers (*Fto$^{-/-}$*) and wild-type mouse livers using RNAzol RT (Molecular Research Center, Inc.). miCLIP was carried out as described previously[24]. RNA-Seq libraries of input and 6mA immunoprecipitated were sequenced in paired-end mode, with 50 bases per read (Illumina HiSeq 2500).

To analyze 6mA coverage at the transcription-start nucleotide (TSN) and internal sites, the following steps were carried out. Input and miCLIP reads were aligned to mm10 with STAR to generate RPM-normalized bedgraphs and sorted bam files[52] (version 2.5.2a;). Bedgraphs were visualized using the Integrative Genomics Viewer[53] (IGV, version 2.4.4). Sorted bam files were converted to bed format and read coverage was determined in a 20-nucleotide window flanking annotated TSN (UCSC) or a 4-nucleotide window flanking the internal site of interest using bedtools (version 2.25.0). miCLIP TSN coverage reads were then counted and normalized to input coverage reads using the Deseq2 pipeline[54] (version 1.18.1; commands: design= ~ assay + condition + assay:condition; test="LRT", reduced= ~ assay + condition). Analysis and visualization was carried out with custom in-house generated R-scripts using RStudio (Version 1.0.136). Only transcripts with normalized read counts > 10 were included in the analyses.

For all other RNA-Seq analyses, total RNA was diluted to a concentration of 50 ng/μl and libraries were prepared using the Illumina TruSeq Stranded mRNA Library Prep Kit (RS-122–2101, Illumina). The libraries were sequenced in paired-end mode, with 100 bases per read. At least two independent biological replicates were sequenced for each condition.

Previously published RNA-Seq datasets utilized in the current study[19,42] were extracted from Gene Expression Omnibus (GEO, NCBI).

Cell culture and animals.

Flp-In T-REx HEK293 cells (R78007, ThermoFisher Scientific) and *DCP2* knockout (*DCP2*^{−/−}) HEK293 cells[19] were maintained in DMEM (ThermoFisher Scientific) with 10% FBS and antibiotics (100 units/ml penicillin and 100 μg/ml of streptomycin) under standard tissue culture conditions.

Control, IDH1[R132H] and IDH2[R140Q] TF-1 erythroleukemia cells were generated and maintained as previously described[36]. Intracellular 2-hydroxyglutarate concentrations were determined as previously described[36]. To inhibit production of neomorphic 2-hydroxyglutarate, IDH1[R132H] cells or IDH2[R140Q] cells were treated for 7 days with 1 μM AGI-5027 (SML1298, Sigma-Aldrich) or AGI-6780 (SML0895, Sigma-Aldrich), respectively.

Naive mouse embryonic stem cells (mESCs) were maintained in Knockout DMEM (ThermoFisher Scientific) with 15% FBS, 100 units/ml penicillin, 100 μg/ml of streptomycin, 2mM L-glutamine, 50 μM β-mercaptoethanol (ThermoFisher Scientific), non-essential amino acids (ThermoFisher Scientific), recombinant mouse LIF (EMD Millipore), GSK3 inhibitor (04000402, Stemgent) and MEK1 inhibitor (04000602, Stemgent) under standard tissue culture conditions. To induce differentiation, naive mESCs were deprived of LIF, GSK3 inhibitor and MEK1 inhibitor for 7 days.

Only male mice *Fto* knockout mice[25] at the age of 12–16 weeks were used. All experiments involving mice were approved by the Institutional Animal Care and Use Committee at Weill Cornell Medicine.

Antibodies.

For western blot analysis mouse α-FTO (ab92821, Abcam) and mouse α-ACTB (A2228, Sigma) were used. For 6mA-immunoprecipitation/miCLIP, rabbit α−6mA (202–003, Synaptic Systems) was used. For SmB-IP, a previously described mouse α-SmB antibody (clone 18F6)[55] was used. For 6mA immunoblotting, a rabbit α−6mA antibody (ab190886, Abcam) was used.

Generation of *FTO* knockout cells.

FTO knockout cells were generated by transfecting Double Nickase plasmids (sc-403708-NIC, Santa Cruz Biotechnology) containing two guide RNAs (Strand A: 5'-CGGTCCCCTGGCCAGTGAAA-3'; Strand B: 5'-CCTGGTGTTCAGGTACTTGT-3') into Flp-In T-REx HEK293 cells (Thermo Fisher Scientific) using LipoD293 (SignaGen Laboratories). 24 hours after transfection, GFP-positive cells were isolated by flow cytometry and reseeded. 48 hours after transfection, cells were subjected to puromycin selection (5 μg/ml) for three days. Cell were then reseeded at a density of 0.5 cells/well in 96-well plates for clonal selection. Loss of FTO protein expression was confirmed by Western blot.

6mA immunoblot.

Denatured small RNA samples (5 μg) were separated by 10% polyacrylamide TBE-Urea denaturing gel electrophoresis at 200 V in 1x TBE. For blotting, separated RNA was transferred onto BrightStar-Plus positive charged nylon membranes (ThermoFisher Scientific) by semidry electroblotting.

After UV crosslinking at 120,000 μJ/cm2 in a Stratalinker UV crosslinker (Stratagene), the membrane was blocked with 1% dry milk powder in PBS-T for 1 h at room temperature and then incubated with the α–6mA (1:500) overnight at 4°C. After washing with PBS-T, membranes were incubated with α-rabbit HRP-conjugated secondary antibody diluted 1:2500 with 1% dry milk powder in PBS-T for 1 h at room temperature. The membrane was visualized by Pierce ECL Western Blotting Substrate (ThermoFisher Scientific) and a Bio-Rad Gel Doc XR system. Band intensity was quantified using Bio-Rad Image Lab software.

Determination of relative m^{6}Am and Am levels in small RNAs by thin layer chromatography.

The m^{6}Am/Am ratio in small RNAs was determined as previously described[19], with some modifications. The small RNA fraction (< 200 nucleotides) was isolated from total RNA using RNAzol RT (Molecular Research Center, Inc.).

For the analysis of individual U-RNAs, the small RNA fraction was separated on 6% TBE-Urea gels, stained with SYBR Gold (ThermoFisher Scientific), and the respective bands (~160 nucleotide for U1 snRNA, and ~180 nucleotides for U2 snRNA) were excised and extracted using ZR small-RNA PAGE Recovery kit (Zymo Research).

200 ng of the small RNA fraction or 40 ng of individual U-RNAs were decapped with 25 units of RppH (NEB) for 3h at 37 °C. The 5' phosphates of the exposed cap-adjacent nucleotide were removed by the addition of 5 units rSAP (NEB) and further incubated for 1 hour at 37°C. All enzymatic reactions were performed in the presence of SUPERase In (ThermoFisher Scientific). After phenol-chloroform extraction and ethanol precipitation, RNA samples were resuspended in 10 μl of DEPC-H$_2$O and 5' ends were labeled using 30 units T4 PNK and 0.8 mBq [γ–^{32}P] ATP at 37°C for 30 min. PNK was heat inactivated at 65°C for 20 min and the reaction was passed through a P-30 spin column (Bio-Rad) to remove unincorporated isotope. The labeled RNA was then digested with 4 units of P1 nuclease (Sigma) for 3h at 37°C.

The nucleotide mixture was subsequently dried using an Eppendorf Vacufuge and reconstituted with 3 μL ddH$_2$O. 1 μl of the released 5' monophosphates from this digest were then analyzed by 2D-TLC on glass-backed PEI-cellulose plates (MerckMillipore) as described previously[19]. Developed TLC plates were imaged as described previously[19].

Protein expression and purification.

Full-length, recombinant human FTO was expressed and purified as previously described[19].

Recombinant human TGS1 (hTGS1) was expressed and purified as previously described[56,57]. Briefly, *E. coli* Tuner cells transformed with pRSET-A-hTGS1$_{618-853}$ were

grown at 37 °C in 2YT medium until OD_{600} of 0.6 and induced with 0.2 mM IPTG. After overnight expression at 18°C, cells were lysed and the protein was purified via Ni-NTA (binding buffer: 50 mM Tris, pH 8, 1 M NaCl, 10 % glycerol; elution buffer: additional 500 mM imidazole) followed by gel filtration (Superdex 75, running buffer: 50 mM Tris, pH 7.5, 200 mM NaCl, 10 % glycerol) to obtain RNase-free protein that was concentrated to ~1.5 mg/mL (MW: 27 kDa), flash frozen and stored at −20°C.

Synthesis and characterization of synthetic oligonucleotides.

Synthetic RNA oligonucleotides were chemically assembled as previously described[19]. To generate $m^{2,2,7}$Gppp-capped oligonucleotides, m^7Gppp-capped synthetic oligonucleotides (ONs) were treated with recombinant human TGS1. For this, reaction mixtures containing 50 mM Tris-HCl (pH 8.0), 5 mM DTT, 50 mM NaCl, 1 mM AdoMet, and 150 μM pure m^7G-ppp-ON (~50 nmoles) and 2.5 μM hTgs1 were incubated at 37°C for 7h. Proteins were removed through a Sep Pak™ C_{18} cartridge. After dilution with 4 mL 100 mM TEAAc, pH 7 the crude mixture was loaded onto the cartridge and washed with 10 mL of 100 mM TEAAc prior to ON elution with 10 mL 50% CH_3CN in 12.5 mM TEAAc. The solution was dried by lyophilization. Remaining AdoMet and the *S*-adenosylhomocysteine (AdoHcy) byproducts were removed as follows: the dry residue was dissolved with 1 mL H_2O and the solution loaded onto a Sephadex G-25 gel filtration cartridge (NAP™–10 cartridge). Elution was performed with 1 mL H_2O. $m^{2,2,7}$Gppp-capped ONs were purified by IEX-HPLC and characterized by mass spectrometry MALDI-TOF as previously described[19].

Measurement of FTO activity.

In vitro demethylation measurements were performed as described previously[19]. Briefly, demethylation activity assay was performed in 20 μl of reaction mixture containing 5 μM synthetic RNA oligonucleotide (either 5'-m^7G-ppp-m^6Am-CACUUGCUUUUGACACAACU-3' or 5'-TMG-ppp-m^6Am-CACUUGCUUUUGACACAACU-3'), 20 nM recombinant, full-length human FTO, 75 mM of $(NH_4)_2Fe(SO_4)_2$, 300 mM alpha-ketoglutarate, 2 mM sodium L-ascorbate, 150 mM KCl and 50 mM HEPES buffer, pH 7.0. The reaction was incubated at 37°C for 10 min and quenched by the addition of 1 mM of EDTA followed by inactivation of the enzyme for 5 min at 95°C.

Sample preparation for HPLC analysis.

After treatment with recombinant, full-length human FTO, oligonucleotides were decapped with 25 units of RppH (NEB) in ThermoPol buffer for 3 h at 37°C. RNA was subsequently digested to single nucleotides with 200 units S1 nuclease (Takara) for 2h at 37°C. 5' phosphates were removed with 5 units rSAP (NEB) for 1h at 37°C. Before loading the samples onto the HPLC column, proteins were removed by size exclusion chromatography with a 10-kDa cut-off filter (VWR).

HPLC analysis of demethylation activity.

The HPLC analysis of nucleosides was performed on an Agilent 1100 system (Agilent Technologies). Separation was performed on a Poroshell 120 EC-C18 column (4μm, 150 ×

4.6 mm, Agilent Technologies) equipped with an EC-C18 Guard cartridge (Agilent Technologies) at 22°C. The mobile phase consisted of buffer A (25 mM NaH_2PO_4) and buffer B (100% acetonitrile). Pump control and peak integration was achieved using the ChemStation software (Rev. A.10.02, build 1757, Agilent Technologies). Retention times of the individual nucleosides were determined with synthetic standards (6.2 min for 2'-*O*-methyladenosine (Am), and 7.2 min for N^6,2'-*O*-dimethyladenosine (m⁶Am).

Sample preparation for mass spectrometry.

To detect cap-dinucleotides by LC-MS/MS, cellular small RNA (0.1–1 μg) was digested with P1 nuclease (0.5–5 units) for 3 hours at 37°C. Proteins were removed by size exclusion chromatography with a 10-kDa cut-off filter (VWR).

The RNA was dried using an Eppendorf Vacufuge and reconstituted with 5 μL ddH₂O. An aliquot was diluted 1:10–1:20 with 80% methanol in ddH₂O. 2 μl of the resulting solution were subjected to LC-MS/MS analysis.

Identification of TMG-ppp-m⁶Am by mass spectrometry.

An aliquot of the $m^{2,2,7}$G-ppp-m⁶Am (TMG-ppp-m⁶Am) standard solution was subjected to LC/MS-MS analysis by an Agilent 1200 LC-system coupled to an Agilent 6538 a quadrupole time-of-flight mass spectrometer equipped with a dual electrospray ionization (ESI) source. A second isocratic pump delivered an internal reference mass solution (ions for negative mode 119.0360 and 966.0007; ions for positive mode 121.0509 and 922.0098) over the second nebulizer into the dual ESI source for continuous calibration during sample analysis. The sample injection volume was 4 μL. Chromatographic separation of the FTO-reaction products was performed using an aqueous normal phase (ANP) column (Cogent™ Diamond Hydride, 4 μm particle size, 150 mm x 2.1 mm; Microsolv Technology Corporation, NJ). The mobile phase consisted of (A) 50% isopropanol with 0.025% acetic acid; and (B) 90% acetonitrile containing 5 mM ammonium acetate. To eliminate the interference of metal ions on the chromatographic peak integrity and ESI ionization, EDTA was added to the mobile phase in a final concentration of 6 μM. The final gradient applied was: 0–1.0 min 99% B, 1.0–7.0 min to 80% B, 7.0–18.0 min to 50% B, 18.0–19.0 min to 0% B and 19.1 to 33.0 min 99% B to regenerate the column. The flow rate was 0.4 mL/min. Positive and negative mass spectra were acquired in the 2 GHz extended dynamic range mode with 1.41 spectra/sec, sampled over a mass/charge range of 50–1000[58]. The operating ESI-source parameters for MS-analysis were: gas temperature 300 °C; drying gas flow 10 L/min; nebulizer pressure 35 psi; TOF capillary voltage 3500 V; fragmentor voltage 140V; skimmer voltage 65 V. Data was processed using Agilent MassHunter Qualitative Analysis Software (B.7. 00 Build 7.0.7024.0, Agilent Technologies).

Analysis of TMG-ppp-m⁶Am and TMG-ppp-Am by mass spectrometry.

Samples were injected into an LC/MS-system comprised of an Agilent 1260 HPLC and an Agilent 6460 triple quadrupole mass spectrometer (Agilent Technologies, Santa Clara, CA) equipped with a JetStream electrospray ionization source, using positive ion-monitoring in multiple reaction monitoring. RNA-caps were resolved on an aqueous normal phase column (Cogent™ Diamond Hydride, 4 μm particle size, 150 mm x 2.1 mm; Microsolv Technology

Corporation, NJ), at a column compartment temperature of 40°C. The samples were maintained at 4°C and the injection volume was 2 μL. The gradient-chromatography previously described by Chen *et al.*[58] was optimized to achieve chromatographic separation of TMG-ppp-m^{6}Am and TMG-ppp-Am. The aqueous mobile phase (A) was 50% isopropanol with 0.025% acetic acid, the organic mobile phase (B) was 90% acetonitrile containing 5 mM ammonium acetate. To eliminate the interference of metal ions on the chromatographic peak integrity and ESI ionization, EDTA was added to the mobile phase in a final concentration of 6 μM. The final gradient applied was: 0–1.0 min 99% B, 1.0–7.0 min to 80% B, 7.0–18.0 min to 50% B, 18.0–19.0 min to 0% B and 19.1 to 29.0 min 99% B to regenerate the column. The flow rate was 0.4 mL/min during data acquisition and 0.6 mL/min during re-equilibration from 21.0 to 28.5 min. Data was saved in centroid mode using Agilent Masshunter workstation acquisition software (B.06.00 Build 6.0.6025.4 SP4). Acquired raw data files were processed with Agilent MassHunter Qualitative Analysis Software (B.07.00 Build 7.0.7024.0, Agilent Technologies). The operating source parameters for MS-analysis were: gas temperature 300°C; gas flow 10 L/min; nebulizer pressure 35 psi; sheath gas temperature 400°C; sheath gas flow 11 L/min; capillary voltage 3500 V; nozzle voltage 0 V; fragmentor voltage 100V; cell accelerator voltage 7 V. Multiple reaction monitoring (MRM) data was acquired for the time segment 10–15 min in which the LC-flow was directed to the MS.

Product ion scans were performed at collision energies of 10, 20, 30, 40, 50 and 60 V, selecting [M+H]$^+$ 843.2 as precursor ion for TMG-ppp-m^{6}Am and [M+H]$^+$ 829.1 for TMG-ppp-Am. Product ions were scanned in an *m/z* range of 50 – 850.

Optimized MRM transitions resulted at a collision energy of 50 eV and represented the deglycosylated base ions: for TMG-ppp-m^{6}Am the transition 843.2→194.1* represented the formation of TMG and 843.2→150.1** the formation of m^{6}Am, accordingly for TMG-ppp-Am 829.1→194.1* represented the formation of TMG and 829.1→136.1** the formation of Am. The transitions 843.2→438.1 and 829.1→424.1 were acquired as additional quality indicator. * indicates quantifier transitions, ** indicates the qualifier transitions.

Immunoprecipitation of spliceosomal complexes.

SmB immunoprecipitations were performed as described previously[39,40]. Briefly, extracts were prepared in ice cold RSB-100 buffer (100 mM NaCl, 10 mM Tris-HCl pH 7.4, 2.5 mM MgCl$_2$) containing 0.1% NP40, protease, phosphatase and RNAse inhibitors, by passing five times through a 26-gauge needle followed by 3 x 5 seconds bursts of sonication on ice and centrifugation at 20,000 x *g* for 15 minutes at 4°C. Extract supernatant was quantified by BCA Assays (ThermoFisher Scientific).

For immunoprecipitation, a mouse monoclonal anti-SmB (18F6) antibody was bound to protein A/G-Sepharose (ThermoFisher Scientific) in RSB-100 buffer containing 0.1% NP40, protease, phosphatase and RNAse inhibitors for 2 hours at 4°C. Following five washes with the same buffer, antibody-bound beads were incubated with 200 μg of cell extract rotating for 2 hours at 4°C. Following five washes, bound RNAs were extracted by treatment with proteinase K (200 μg) for 20 minutes at 37°C followed by TRIzol LS (ThermoFisher Scientific) extraction. Immunoprecipitated RNA was then analyzed by TLC.

Alternative splicing analysis.

For alternative splicing analysis, paired reads were aligned to the human transcriptome (hg19) or mouse transcriptome (mm10) using STAR[52] (v020201). Biological replicates were then merged and indexed using samtools (v1.5). The module exon_utils from the MISO package[59] was used to extract the constitutive exons from the transcriptome annotation (iGenomes, UCSC build hg19). The resulting annotations were then used in conjunction with the pe_utils module (MISO) to estimate fragment length distribution. The MISO package was then used to quantify percent spliced-in values (PSI) for each splicing event annotated for hg19 (pre-built MISO annotations). We used skipped exons (SE) as well as alternatively spliced first and last exons (A5SS and A3SS). We then used MISO to compare changes in splicing events, which reports the change in PSI values as well as the associated Bayes factor. For motif analysis, we extracted the included exons along with 250nt flanking sequences. We then used FIRE[51], in non-discovery mode, to ask whether the presence or absence of known splicing regulator-binding sites[60] were significantly associated with changes in PSI values. In addition to enrichment profiles among the down- or up-regulated exons, FIRE also provides the mutual information (MI) values and associated z-scores and robustness scores.

Northern blot.

500 ng total RNA extracted from wild type and $DCP^{-/-}$ HEK293T cells was run on a 10% TBE-Urea gel (ThermoFisher). RNA was subsequently transferred onto the BrightStar-Plus nylon membrane (ThermoFisher). The transferred RNA was UV-crosslinked twice with 0.12 J/cm^2. The membrane was prehybridized in 20 mL ULTRAHyb-Oligo buffer (ThermoFisher) at 42°C for an hour. 10 nM (final) 3'-biotinylated DNA probe for snRNAs and 5.8 S rRNA (loading control) were incubated at 42°C overnight. The membrane was washed twice (20 min each) in a buffer containing 2x SSC and 0.5% SDS. Detection was performed using Chemiluminescent Nucleic Acid Detection Module (ThermoFisher) according to the manufacturer's instructions.

U2 snRNA probe: 5'-TACTGCAATACCAGGTCGATGCGT-Biotin-3'

U5 snRNA probe: 5'-GACTCAGAGTTGTTCCTCTCCACG-Biotin-3'

5.8S rRNA probe: 5'-AGACAGGCGTAGCCCCGGGAGGAA-Biotin-3'

Classification of mRNAs based on the first nucleotide.

Annotated TSS were extracted from UCSC table browser. A complete list of transcription start sites is found in the Supplementary Information Table 1.

Statistics and software.

P-values were calculated with a two-tailed unpaired Student's *t*-test or, for the comparison of more than two groups, with a one- or two-way ANOVA followed by Tukey's post-test. *P*-values of 0.05 or less were considered significant.

Supplementary Material

Refer to Web version on PubMed Central for supplementary material.

Acknowledgements

References:

1. Hadjiolov AA, Venkov PV & Tsanev RG Ribonucleic acids fractionation by density-gradient centrifugation and by agar gel electrophoresis: a comparison. Anal Biochem 17, 263–267 (1966). [PubMed: 5339429]

2. Dreyfuss G, Philipson L & Mattaj IW Ribonucleoprotein particles in cellular processes. J Cell Biol 106, 1419–1425 (1988). [PubMed: 2836428]

3. Lührmann R Functions of U-snRNPs. Mol Biol Rep 14, 183–192 (1990). [PubMed: 2141907]

4. Kunkel GR, Maser RL, Calvet JP & Pederson T U6 small nuclear RNA is transcribed by RNA polymerase III. Proc Natl Acad Sci U S A 83, 8575–8579 (1986). [PubMed: 3464970]

5. Dahlberg JE & Lund E Structure and expression of U-snRNA genes. Mol Biol Rep 12, 139–143 (1987). [PubMed: 3316972]

6. Baillat D et al. Integrator, a multiprotein mediator of small nuclear RNA processing, associates with the C-terminal repeat of RNA polymerase II. Cell 123, 265–276, doi:10.1016/j.cell.2005.08.019 (2005). [PubMed: 16239144]

7. Cory S & Adams JM Modified 5'-termini in small nuclear RNAs of mouse myeloma cells. Mol Biol Rep 2, 287–294 (1975). [PubMed: 1214781]

8. Busch H, Reddy R, Rothblum L & Choi YC SnRNAs, SnRNPs, and RNA processing. Annu Rev Biochem 51, 617–654, doi:10.1146/annurev.bi.51.070182.003153 (1982). [PubMed: 6180681]

9. Mattaj IW Cap trimethylation of U snRNA is cytoplasmic and dependent on U snRNP protein binding. Cell 46, 905–911 (1986). [PubMed: 2944599]

10. Matera AG & Wang Z A day in the life of the spliceosome. Nat Rev Mol Cell Biol 15, 108–121, doi:10.1038/nrm3742 (2014). [PubMed: 24452469]

11. Pellizzoni L Chaperoning ribonucleoprotein biogenesis in health and disease. EMBO Rep 8, 340–345, doi:10.1038/sj.embor.7400941 (2007). [PubMed: 17401408]

12. Patel SB & Bellini M The assembly of a spliceosomal small nuclear ribonucleoprotein particle. Nucleic Acids Res 36, 6482–6493, doi:10.1093/nar/gkn658 (2008). [PubMed: 18854356]

13. Shukla S & Parker R Quality control of assembly-defective U1 snRNAs by decapping and 5'-to-3' exonucleolytic digestion. Proc Natl Acad Sci U S A 111, E3277–3286, doi:10.1073/pnas. 1412614111 (2014). [PubMed: 25071210]

14. Ishikawa H et al. Identification of truncated forms of U1 snRNA reveals a novel RNA degradation pathway during snRNP biogenesis. Nucleic Acids Res 42, 2708–2724, doi:10.1093/nar/gkt1271 (2014). [PubMed: 24311566]

15. Karijolich J & Yu YT Spliceosomal snRNA modifications and their function. RNA Biol 7, 192–204 (2010). [PubMed: 20215871]

16. Pendleton KE et al. The U6 snRNA m(6)A Methyltransferase METTL16 Regulates SAM Synthetase Intron Retention. Cell 169, 824–835.e814, doi:10.1016/j.cell.2017.05.003 (2017). [PubMed: 28525753]

17. Jia G et al. N6-methyladenosine in nuclear RNA is a major substrate of the obesity-associated FTO. Nat Chem Biol 7, 885–887, 10.1038/nchembio.687 (2011). [PubMed: 22002720]

18. Jia G et al. Oxidative demethylation of 3-methylthymine and 3-methyluracil in single-stranded DNA and RNA by mouse and human FTO. FEBS Letters 582, 3313–3319, doi:10.1016/j.febslet. 2008.08.019 (2008). [PubMed: 18775698]

19. Mauer J et al. Reversible methylation of m(6)Am in the 5' cap controls mRNA stability. Nature 541, 371–375, doi:10.1038/nature21022 (2017). [PubMed: 28002401]

20. Wei C, Gershowitz A & Moss B N6, O2'-dimethyladenosine a novel methylated ribonucleoside next to the 5' terminal of animal cell and virus mRNAs. Nature 257, 251–253 (1975). [PubMed: 1161029]

21. Kruse S et al. A novel synthesis and detection method for cap-associated adenosine modifications in mouse mRNA. Scientific Reports 1, doi:10.1038/srep00126 (2011).

22. Hess ME et al. The fat mass and obesity associated gene (Fto) regulates activity of the dopaminergic midbrain circuitry. Nat Neurosci 16, 1042–1048, 10.1038/nn.3449 (2013). [PubMed: 23817550]

23. Reddy R, Henning D, Epstein P & Busch H Primary and secondary structure of U2 snRNA. Nucleic Acids Res 9, 5645–5658 (1981). [PubMed: 6796940]

24. Linder B et al. Single-nucleotide-resolution mapping of m6A and m6Am throughout the transcriptome. Nat Methods 12, 767–772, doi:10.1038/nmeth.3453 (2015). [PubMed: 26121403]

25. Fischer J et al. Inactivation of the Fto gene protects from obesity. Nature 458, 894–898, doi:10.1038/nature07848 (2009). [PubMed: 19234441]

26. Mowry KL & Steitz JA Identification of the human U7 snRNP as one of several factors involved in the 3' end maturation of histone premessenger RNA's. Science 238, 1682–1687 (1987). [PubMed: 2825355]

27. Jawdekar GW & Henry RW Transcriptional regulation of human small nuclear RNA genes. Biochim Biophys Acta 1779, 295–305, doi:10.1016/j.bbagrm.2008.04.001 (2008). [PubMed: 18442490]

28. Bohnsack MT & Sloan KE Modifications in small nuclear RNAs and their roles in spliceosome assembly and function. Biol Chem 399, 1265–1276, doi:10.1515/hsz-2018-0205 (2018). [PubMed: 29908124]

29. Wei J et al. Differential m6A, m6Am, and m1A Demethylation Mediated by FTO in the Cell Nucleus and Cytoplasm. Mol Cell 71, 973–985.e975, doi:10.1016/j.molcel.2018.08.011 (2018). [PubMed: 30197295]

30. Hogeweg P & Konings DA U1 snRNA: the evolution of its primary and secondary structure. J Mol Evol 21, 323–333 (1984). [PubMed: 6443312]

31. Bringmann P & Luhrmann R Antibodies specific for N6-methyladenosine react with intact snRNPs U2 and U4/U6. FEBS Lett 213, 309–315, doi:0014-5793(87)81512-0 [pii] (1987). [PubMed: 2951275]

32. Yang Y et al. UOK 262 cell line, fumarate hydratase deficient (FH-/FH-) hereditary leiomyomatosis renal cell carcinoma: in vitro and in vivo model of an aberrant energy metabolic pathway in human cancer. Cancer Genet Cytogenet 196, 45–55, doi:10.1016/j.cancergencyto.2009.08.018 (2010). [PubMed: 19963135]

33. McDonough MA, Farooqi IS, Lindahl T, Ashcroft FM & Schofield CJ The obesity-associated FTO gene encodes a 2-oxoglutarate-dependent nucleic acid demethylase. Science (New York, NY) 318, 1469–1472, doi:10.1126/science.1151710 (2007).

34. Aik W et al. Structural basis for inhibition of the fat mass and obesity associated protein (FTO). J Med Chem 56, 3680–3688, doi:10.1021/jm400193d (2013). [PubMed: 23547775]

35. Ward PS et al. The common feature of leukemia-associated IDH1 and IDH2 mutations is a neomorphic enzyme activity converting alpha-ketoglutarate to 2-hydroxyglutarate. Cancer Cell 17, 225–234, doi:10.1016/j.ccr.2010.01.020 (2010). [PubMed: 20171147]

36. Wang F et al. Targeted inhibition of mutant IDH2 in leukemia cells induces cellular differentiation. Science (New York, NY) 340, 622–626, doi:10.1126/science.1234769 (2013).

37. Rohle D et al. An inhibitor of mutant IDH1 delays growth and promotes differentiation of glioma cells. Science (New York, NY) 340, 626–630, doi:10.1126/science.1236062 (2013).

38. Bennett Saidu NE et al. Dimethyl fumarate is highly cytotoxic in KRAS mutated cancer cells but spares non-tumorigenic cells. Oncotarget 9, 9088–9099, doi:10.18632/oncotarget.24144 (2018). [PubMed: 29507676]

39. Gabanella F et al. Ribonucleoprotein assembly defects correlate with spinal muscular atrophy severity and preferentially affect a subset of spliceosomal snRNPs. PLoS One 2, e921, doi: 10.1371/journal.pone.0000921 (2007). [PubMed: 17895963]

40. Lotti F et al. An SMN-dependent U12 splicing event essential for motor circuit function. Cell 151, 440–454, doi:10.1016/j.cell.2012.09.012 (2012). [PubMed: 23063131]

41. Zhao X et al. FTO-dependent demethylation of N6-methyladenosine regulates mRNA splicing and is required for adipogenesis. Cell Research 24, 1403–1419, doi:papers2://publication/doi/ 10.1038/cr.2014.151 (2014). [PubMed: 25412662]

42. Bartosovic M et al. N6-methyladenosine demethylase FTO targets pre-mRNAs and regulates alternative splicing and 3'-end processing. Nucleic Acids Res 45, 11356–11370, doi:10.1093/nar/ gkx778 (2017). [PubMed: 28977517]

43. Wei J et al. Differential m(6)A, m(6)Am, and m(1)A Demethylation Mediated by FTO in the Cell Nucleus and Cytoplasm. Mol Cell 71, 973–985 e975, doi:10.1016/j.molcel.2018.08.011 (2018). [PubMed: 30197295]

44. Su R et al. R-2HG Exhibits Anti-tumor Activity by Targeting FTO/m(6)A/MYC/CEBPA Signaling. Cell 172, 90–105 e123, doi:10.1016/j.cell.2017.11.031 (2018). [PubMed: 29249359]

45. Ke S et al. m(6)A mRNA modifications are deposited in nascent pre-mRNA and are not required for splicing but do specify cytoplasmic turnover. Genes Dev 31, 990–1006, doi:10.1101/gad. 301036.117 (2017). [PubMed: 28637692]

46. Pomeranz Krummel DA, Oubridge C, Leung AK, Li J & Nagai K Crystal structure of human spliceosomal U1 snRNP at 5.5 A resolution. Nature 458, 475–480, doi:10.1038/nature07851 (2009). [PubMed: 19325628]

47. Fury MG & Zieve GW U6 snRNA maturation and stability. Exp Cell Res 228, 160–163, doi: 10.1006/excr.1996.0311 (1996). [PubMed: 8892983]

48. Dvinge H RNA components of the spliceosome regulate tissue- and cancer-specific alternative splicing. bioRxiv, doi:10.1101/326983 (2018).

49. Zhang Z et al. SMN deficiency causes tissue-specific perturbations in the repertoire of snRNAs and widespread defects in splicing. Cell 133, 585–600, doi:10.1016/j.cell.2008.03.031 (2008). [PubMed: 18485868]

50. Kaida D et al. U1 snRNP protects pre-mRNAs from premature cleavage and polyadenylation. Nature 468, 664–668, doi:10.1038/nature09479 (2010). [PubMed: 20881964]

Methods References:

51. Elemento O, Slonim N & Tavazoie S A universal framework for regulatory element discovery across all genomes and data types. Mol Cell 28, 337–350, 10.1016/j.molcel.2007.09.027 (2007). [PubMed: 17964271]

52. Dobin A et al. STAR: ultrafast universal RNA-seq aligner. Bioinformatics 29, 15–21, doi:10.1093/ bioinformatics/bts635 (2013). [PubMed: 23104886]

53. Robinson JT et al. Integrative genomics viewer. Nat Biotechnol 29, 24–26, doi:10.1038/nbt.1754 (2011). [PubMed: 21221095]

54. Love MI, Huber W & Anders S Moderated estimation of fold change and dispersion for RNA-seq data with DESeq2. Genome Biol 15, 550, doi:10.1186/s13059-014-0550-8 (2014). [PubMed: 25516281]

55. Carissimi C, Saieva L, Gabanella F & Pellizzoni L Gemin8 is required for the architecture and function of the survival motor neuron complex. J Biol Chem 281, 37009–37016, doi:10.1074/ jbc.M607505200 (2006). [PubMed: 17023415]

56. Monecke T, Dickmanns A & Ficner R Structural basis for m7G-cap hypermethylation of small nuclear, small nucleolar and telomerase RNA by the dimethyltransferase TGS1. Nucleic Acids Res 37, 3865–3877, doi:10.1093/nar/gkp249 (2009). [PubMed: 19386620]

57. Schulz D & Rentmeister A An enzyme-coupled high-throughput assay for screening RNA methyltransferase activity in E. coli cell lysate. RNA Biol 9, 577–586, doi:10.4161/rna.19818 (2012). [PubMed: 22614835]

58. Chen Q et al. Untargeted plasma metabolite profiling reveals the broad systemic consequences of xanthine oxidoreductase inactivation in mice. PLoS One 7, e37149, doi:10.1371/journal.pone. 0037149 (2012). [PubMed: 22723833]

59. Katz Y, Wang ET, Airoldi EM & Burge CB Analysis and design of RNA sequencing experiments for identifying isoform regulation. Nat Methods 7, 1009–1015, doi:10.1038/nmeth.1528 (2010). [PubMed: 21057496]

60. Ray D et al. A compendium of RNA-binding motifs for decoding gene regulation. Nature 499, 172–177, 10.1038/nature12311 (2013). [PubMed: 23846655]
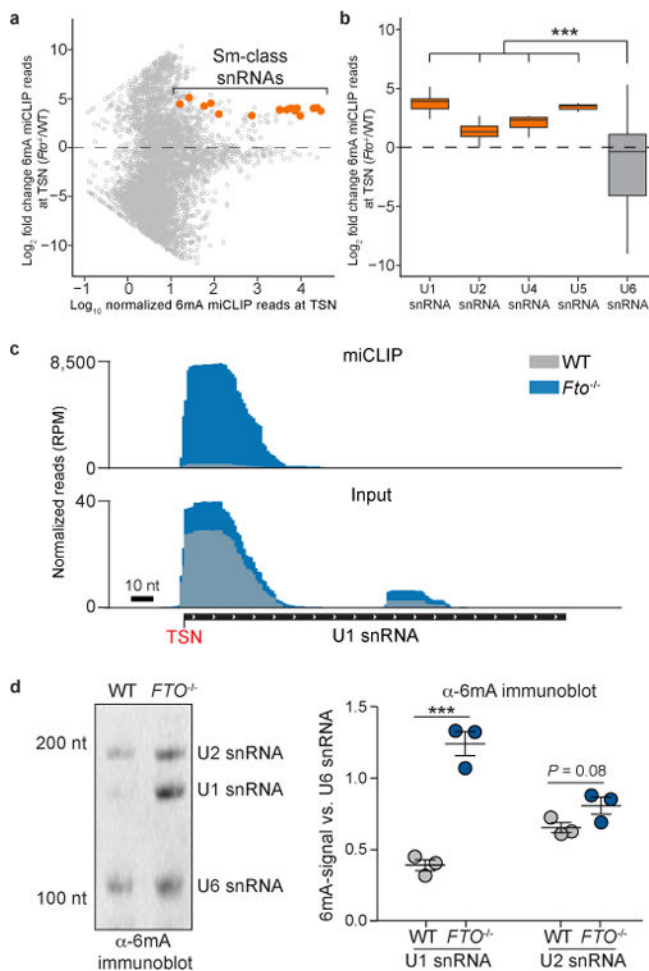
Figure 1 |. FTO selectively demethylates small nuclear RNAs.

a, N^6-methyladenine (6mA) mapping in total RNA using miCLIP reveals FTO-dependent demethylation of small nuclear RNAs (snRNAs). Shown is the $\log_2$ fold-change in methylation of *Fto* knockout mouse liver ($Fto^{-/-}$) compared to wild-type liver (WT). Transcripts with significant upregulation ($P < 0.05$) of transcription-start nucleotide (TSN) methylation are indicated in orange (data represents average from datasets of three independent biological replicates per genotype). **b,** FTO deficiency leads to increased TSN methylation of major spliceosomal snRNAs. The mean $\log_2$ fold-change in TSN methylation of specific snRNA gene classes (U1, U2, U4, U5 and U6) in $Fto^{-/-}$ mouse liver compared to WT is shown (data represents average from datasets of three independent biological replicates per genotype; each box shows the first quartile, median, and third quartile; whiskers represent $1.5 \times$ interquartile ranges; one-way ANOVA with Tukey's post hoc test ****P < 0.001*). **c**, U1 snRNA shows increased TSN methylation in FTO-deficient mouse liver. Grey tracks denote WT liver, blue tracks denote $Fto^{-/-}$ liver. A representative read coverage track for U1 snRNA is shown (RPM = reads per million mapped reads; data represents combined tracks from datasets of three independent biological replicates per genotype). **d**, FTO deficiency leads to increased methylation of mature snRNAs. 6mA-immunoblot of WT and $FTO^{-/-}$ HEK293 cells. Methylation of U1, U2, and U6 snRNAs was detected with an

antibody directed against 6mA. The left panel shows a representative 6mA-immunoblot with positions of nucleotide size markers and individual snRNAs indicated on the left and right, respectively. The right panel shows the quantification of 6mA signal in U1 and U2 snRNA relative to the 6mA signal in U6 snRNA (n=3 independent biological replicates; mean ±s.e.m.; unpaired student's *t*-test ****P 0.001*).
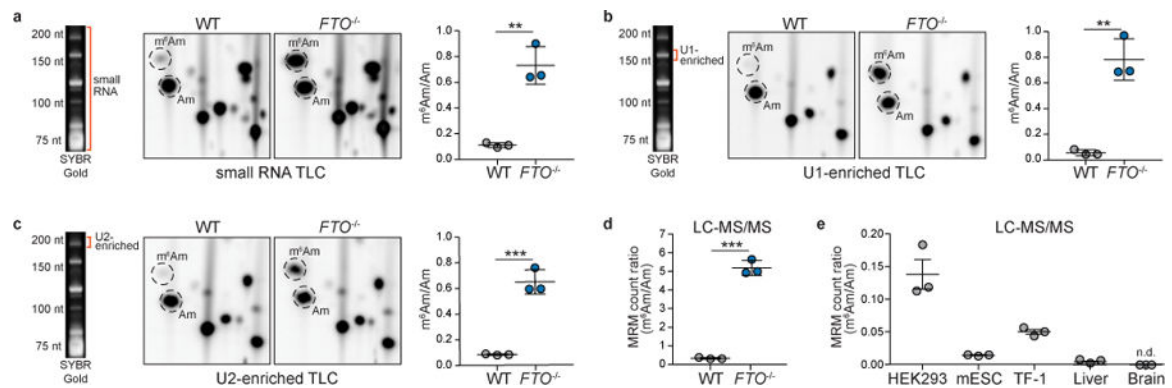
Figure 2 |. Reversible N^6,2'-O-dimethyladenosine (m^{6}Am) in small nuclear RNAs.

a, FTO deficiency reveals the presence of m^{6}Am in small RNAs. Modified adenosines in snRNA caps from wild-type (WT) and FTO-deficient ($FTO^{-/-}$) HEK293 cells were analyzed by thin-layer chromatography (TLC). The migration position of m^{6}Am and 2'-O-methyladenosine (Am) is indicated by dashed circles. Orange line indicates the small RNA fraction (RNAs<200 nt) used for analysis. Right panel shows quantification of m^{6}Am/Am ratios in small RNA (n=3 independent biological replicates; mean±s.d; unpaired student's t-test **P 0.01). **b**, FTO deficiency reveals the presence of m^{6}Am in U1 snRNA. m^{6}Am and Am in U1 snRNA caps from WT and $FTO^{-/-}$ HEK293 cells were analyzed by TLC. The migration position of m^{6}Am and 2'-O-methyladenosine (Am) is indicated by the dashed black circles. Right panel shows the quantification of the m^{6}Am/Am ratio in the U1-enriched fraction (n=3 independent biological replicates; mean±s.d; unpaired student's t-test **P 0.01). **c**, FTO deficiency reveals the presence of m^{6}Am in U2 snRNA. The relative abundance of m^{6}Am and Am in U2 snRNA caps from WT and $FTO^{-/-}$ HEK293 cells was determined by TLC. (n=3 independent biological replicates; mean±s.d; unpaired student's t-test ***P 0.001). **d**, FTO deficiency increases the relative abundance of m$_2$-snRNA caps. The extended cap structure dinucleotide of small RNA from WT and $FTO^{-/-}$ HEK293 cells was analyzed by LC-MS/MS. Shown is the ratio of m$_2$-snRNA caps (m^{6}Am) to m$_1$-snRNA caps (Am) (n=3 independent biological replicates, mean±s.d.; unpaired Student's t-test, ***P< 0.001). **e**, Differential expression of m$_2$-snRNA (cap-ppp-m^{6}Am) caps across cells and tissues. The extended cap structure dinucleotide of small RNA from wild-type HEK293 cells, naïve mouse embryonic stem cells (mESCs), TF-1 erythroleukemia cells, as well as mouse liver and brain tissue was analyzed by LC-MS/MS. Shown is the ratio of m$_2$-snRNA caps to m$_1$-snRNA caps (n.d.=cap-ppp-m^{6}Am not detected; n=3 independent biological replicates, mean±s.d.; unpaired Student's t-test, ** P<0.01).

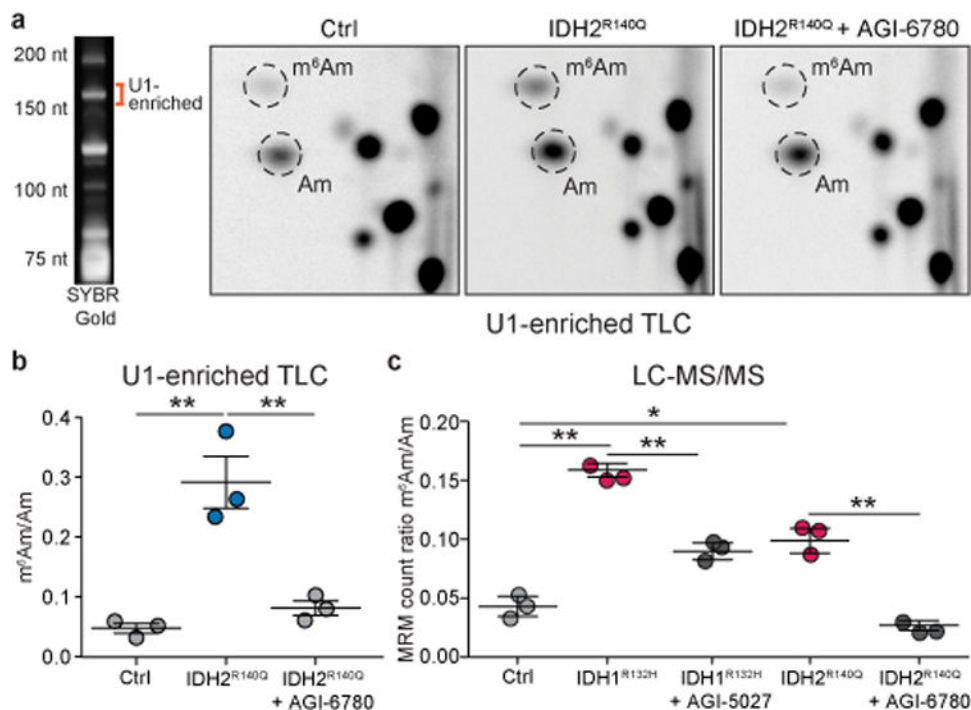**Figure 3 |. m$_2$-snRNAs are reversibly regulated in oncometabolite-dependent cancer models.**
a, Mutant IDH2 increases the abundance of m^{6}Am caps in U1 snRNA. Gel-extracted U1 snRNA from Ctrl and mutant IDH2^{R140Q}-expressing TF-1 cells was analyzed by thin-layer chromatography (TLC). The migration position of m^{6}Am and 2'-O-methyladenosine (Am) is indicated by dashed circles. Orange line indicates the small RNA fraction (RNAs<200 nt) used for analysis. Specific inhibition of mutant IDH2 (AGI-6780) isoforms shows that these effects are reversible by blocking production of 2-HG. Representative images are shown. **b**, Increased abundance of m^{6}Am caps in U1 snRNA of oncometabolite-dependent cancer cells. Shown is the quantification m^{6}Am/Am ratios in U1 snRNA from Ctrl and mutant IDH2^{R140Q}-expressing TF-1 cells as measured by TLC (n=3 independent biological replicates, mean±s.d.; unpaired Student's t-test, **P<0.01). **c**, Increased abundance of m$_2$-snRNA caps in oncometabolite-dependent cancer. The extended cap structure dinucleotide of small RNA from Ctrl, mutant IDH1^{R132H}-, and mutant IDH2^{R140Q}-expressing TF-1 cells was analyzed by LC-MS/MS. Shown is the ratio of m$_2$-snRNA caps (m^{6}Am) to m$_1$-snRNA caps (Am) represented by the integrated peak area ratio of the MRM transition. Blocking production of 2-HG by specific inhibition of mutant IDH1 and IDH2 isoforms with AGI-5027 and AGI-6780, respectively, shows that these effects are reversible (n=3 independent biological replicates, mean±s.d.; one-way ANOVA with Tukey's post hoc test *P 0.05, **P 0.01).
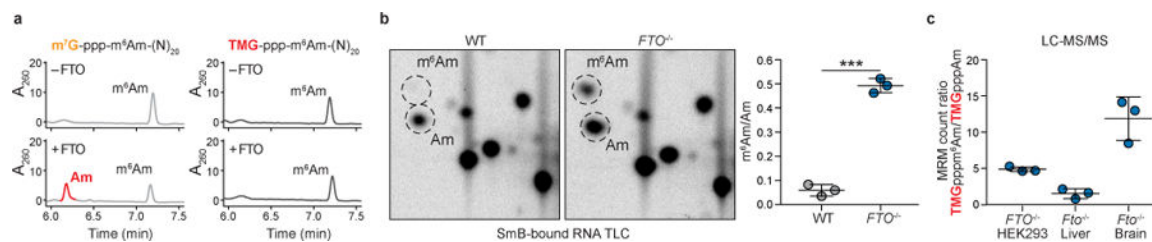
Figure 4 |. m₂-snRNAs are incorporated into snRNPs.

a, FTO does not exhibit measurable demethylation of m^{6}Am in RNA containing a $N^{2,2,7}$-trimethylguanosine (TMG) cap. To determine whether FTO demethylates mature snRNA, we incubated full-length human FTO with synthetic 20-mer RNA oligonucleotides starting either with a 5'-m^{7}G-ppp-m^{6}Am or 5'-TMG-ppp-m^{6}Am cap. In the context of an m^{7}G cap, FTO readily converted m^{6}Am to Am (left panels). However, the presence of an TMG cap completely blocked FTO demethylation activity towards m^{6}Am (right panels), indicating that snRNAs starting with a TMG-ppp-m^{6}Am are not a physiological target of FTO (representative HPLC track shown; *n*=3 independent experiments). **b,** m₂-snRNAs are incorporated into small nuclear ribonucleoproteins (snRNPs). To test whether m₂-snRNAs are incorporated into snRNPs, immunoprecipitation of the SmB spliceosomal protein was performed. The relative abundance of modified adenosines in SmB-bound small RNA caps derived from wild-type (WT) and FTO-deficient (*FTO*$^{-/-}$) HEK293 cells was determined by thin-layer chromatography. The left panel shows a representative image of the migration pattern of radiolabeled nucleotides, where the position of m^{6}Am and Am is indicated by the dashed black circles. The right panel shows the quantification of the m^{6}Am/Am ratio in small RNA (*n*=3 independent biological replicates; mean ± s.d; unpaired student's *t*-test ***P 0.001). **c,** m₂-snRNAs have TMG caps. We asked if the presence of m^{6}Am in snRNA blocks the maturation of the snRNA cap from m^{7}G to TMG. The extended cap structure dinucleotide of small RNA from FTO-deficient HEK293 cells and tissues was analyzed by LC-MS/MS. Shown is the ratio of m₂-snRNA TMG caps to m₁-snRNA. TMG-capped snRNAs were readily detected in HEK293 cells, as well as in mouse liver and brain tissue, demonstrating that, similar to m₁-snRNAs, m₂-snRNAs are subjected to m^{7}G cap hypermethylation (n=3 independent biological replicates, mean ± s.d.).